MCP Papers in Press. Published on March 9, 2018 as Manuscript RA117.000052

Protease activities triggered by *Ralstonia solanacearum* infection in susceptible and tolerant tomato lines

Marc Planas-Marquès[1,2], Martí Bernardo-Faura[1], Judith Paulus[3], Farnusch Kaschani[4], Markus Kaiser[4], Marc Valls[1,2*], Renier A. L. van der Hoorn[3] and Núria S. Coll[1*]

[1] Centre for Research in Agricultural Genomics (CRAG), CSIC-IRTA-UAB-UB, Campus UAB, Bellaterra, 08193 Barcelona, Catalonia, Spain.

[2] Department of Genetics, University of Barcelona, 08028 Barcelona, Catalonia, Spain.

[3] Plant Chemetics Laboratory, Department of Plant Sciences, University of Oxford, South Parks Road, OX1 3RB Oxford, UK;

[4] Chemische Biologie, Zentrum für Medizinische Biotechnologie, Fakultät für Biologie, Universität Duisburg-Essen, Universitätsstr. 2, 45117 Essen, Germany.

[*]Authors for correspondence:

Nuria S. Coll

e-mail: nuria.sanchez-coll@cragenomica.es

Telephone: +34 93 5606600

Fax: +34 93 5606601

Marc Valls

e-mail: marcvalls@ub.edu

Telephone: +34 93 4021496

Fax: +34 93 4034420

Running title: Active tomato proteases upon *R. solanacearum* infection

Abbreviations: Activity-based protein profiling (ABPP), Papain-like Cysteine Protease (PLCP), Pectinacetylesterase (PAE), *Phytophthora* inhibited protease 1 (Pip1), Quantitative Trait Locus (QTL), Required for *C. fulvum* resistance 3 (Rcr3), Serine Carboxypeptidases (SCP), Serine Hydrolase (SH), Subtilisin-like Protease (SLP).

Key words: Activity-based protein profiling, bacterial wilt, disease resistance, papain-like cysteine protease, proteomics, *Ralstonia solanacearum*, serine hydrolase, tomato.

Word count (main body): 7651

Number of figures: 5 (color figures 1, 3, 4 and 5)

Supplementary data: Tables S1 to S4, Figures S1 to S8

Summary

Activity-based protein profiling (ABPP) is a powerful proteomic technique to display protein activities in a proteome. It is based on the use of small molecular probes that react with the active site of proteins in an activity-dependent manner. We used ABPP to dissect the protein activity changes that occur in the intercellular spaces of tolerant (Hawaii 7996) and susceptible (Marmande) tomato plants in response to *R. solanacearum*, the causing agent of bacterial wilt, one of the most destructive bacterial diseases in plants. The intercellular space –or apoplast– is the first battlefield where the plant faces *R. solanacearum*. Here, we explore the possibility that the limited *R. solanacearum* colonization reported in the apoplast of tolerant tomato is partly determined by its active proteome. Our work reveals specific activation of papain-like cysteine proteases (PLCPs) and serine hydrolases (SHs) in the leaf apoplast of the tolerant tomato Hawaii 7996 upon *R. solanacearum* infection. In particular, the P69 family members P69C and P69F, and an unannotated lipase (Solyc02g077110.2.1), were found to be post-translationally activated. In addition, protein network analysis showed that deeper changes in network topology take place in the susceptible tomato variety, suggesting that the tolerant cultivar might be more prepared to face *R. solanacearum* in its basal state. Altogether this work identifies significant changes in the activity of 4 PLCPs and 27 SHs in the tomato leaf apoplast in response to *R. solanacearum*, most of which are yet to be characterized. Our findings denote the importance of novel proteomic approaches such as ABPP to provide new insights on old and elusive questions regarding the molecular basis of resistance to *R. solanacearum*.

Introduction

Bacterial wilt caused by the soil-borne pathogen *Ralstonia solanacearum* is one of the most destructive and economically damaging bacterial diseases, affecting over 200 plant species, including important crops such as tomato, potato and peanut (1, 2). Yield losses caused by *R. solanacearum* on tomato can reach up to 90% in some countries (3).

Management of bacterial wilt remains difficult due to *R. solanacearum* aggressiveness, its broad geographical distribution and its long persistence in soil and water (1, 4). Historically, grafting approaches using tolerant cultivars as rootstocks have been the most effective method to control bacterial wilt (5–7). In tomato, the Hawaii cultivar series –particularly Hawaii 7996– has been proven to be the most effective source of resistance against various *R. solanacearum* strains under different environmental conditions (8–10). In *Arabidopsis thaliana*, two major resistance genes, RRS1-R (Resistance to *Ralstonia solanacearum* 1) and RPS4 (Resistance to *Pseudomonas syringae* 4), were shown to provide resistance to *R. solanacearum* as a dual *R*-gene system, recognizing the type III effector PopP2 and triggering defense (11–14). However, no major *R*-genes have been identified in tomato (15), where resistance has been reported to be mainly quantitative, involving two major Quantitative Trait Loci (QTLs) (*Bwr-12* and *Bwr-6*), and three minor loci (*Bwr-3*, *Bwr-4* and 8 *Bwr-8*) (16–21). These QTLs, defined in the cultivar Hawaii 7996, were found to be both strain- and environment-specific (16, 21).

R. solanacearum infects plants through wounds in the roots, at secondary root emerging sites and at root tips, and migrates intercellularly through the apoplast until it reaches the xylem vessels, where it multiplies and spreads systemically (4, 22). More than two decades ago,

Grimault & Prior (23), and later on McGarvey & collaborators (24), reported limited bacterial growth in the root, collar and middle stem of tolerant tomato cultivars. Hawaii 7996 showed the least bacterial colonization, and immunostaining analysis demonstrated lower levels of bacteria in the root apoplast (24). Later studies pointed to the importance of physical barriers and intercellular spaces in tomato defense against *R. solanacearum* (25–27) but a deep understanding of the molecular mechanisms involved in resistance is still lacking. The apoplast is thus the first battlefield where the plant has to face the pathogen before it reaches the xylem. In this narrow compartment both plants and pathogens secrete a diverse set of molecules that ultimately determine the outcome of the infection. Recent research provides evidence of plant apoplastic proteases playing an important role in immunity, with their activity often targeted by pathogen-derived effectors (28, 29).

In this study we explore the possibility that the limited *R. solanacearum* colonization of intercellular spaces depicted by tolerant tomato cultivars (24, 27) is partly determined by the molecular environment of their apoplast. In particular, we have dissected the dynamic changes in protein activities that take place in the apoplast of tolerant (Hawaii 7996) and susceptible (Marmande) tomato in response to *R. solanacearum* using activity-based protein profiling (ABPP). ABPP is a technique that identifies the active proteins in a proteome. It is based on the use of small labelled molecules that react with the active site of proteins in an activity-dependent manner (30, 31).

ABPP has made important contributions to the understanding of immune responses in plants, allowing the identification of differential activities at the plant-pathogen interface (32). Changes in the activities of the papain-like cysteine protease (PLCPs) and the serine hydrolase (SH) protease families are of particular interest, since they have been reported in

the apoplast of tomato and other plant-pathogen systems (reviewed by Kołodziejek & van der Hoorn) (32). PLCPs are usually 23-30 kDa in size, and use a catalytic cysteine residue to cleave peptide bonds in protein substrates. They have been shown to be required for full plant resistance against various bacterial, fungal, and oomycete pathogens, inducing a broad spectrum of defense (33). Some PLCPs are required for defense-related program cell death, like the protease cathepsin B from *Nicotiana Benthamiana*. Silencing of cathepsin B prevented cell death and compromised non-host disease resistance caused by *Erwinia amylovora* and *Pseudomonas syringae* pv. *tomato* (34). PLCPs can also act as co-receptors in the recognition of pathogen effectors. This is the case of Rcr3 (Required for *Cladosporium fulvum* Resistance 3), which is required by the tomato receptor-like protein Cf-2 for the perception of the *Cladosporium fulvum* effector Avr2 (35) or the allergen-like effector protein Gr-VAP1 from the potato cyst nematode *Globodera rostochiensis* (36), acting as a decoy and hence triggering cell death. SHs, on the other hand, comprise a large collection of enzymes from different structural classes that carry an activated serine residue in their catalytic site. SHs fulfill diverse biochemical roles and are involved in a wide range of physiological processes including plant immunity (37). In addition, members of the PLCP and SH protease families have been shown to be up-regulated upon pathogen infection or targeted by pathogen-derived inhibitors (29).

The aim of this work was to identify the active apoplastic proteases involved in the *R. solanacearum* infection of tomato. We describe a variety-specific induction of PLCP and SH protein activities in response to *R. solanacearum*. Altogether this work denotes the importance of novel proteomic approaches –such as ABPP– to provide new insights on old questions regarding the molecular basis of resistance to bacterial wilt.

Experimental Procedures

Bacterial strains and culture conditions

All assays were performed using a *Ralstonia solanacearum* GMI1000 (Phylotype I, race 1 biovar 3) reporter strain carrying the *luxCDABE* operon under the constitutive promoter PpsbA integrated in its chromosome. *R. solanacearum* was routinely grown at 28ºC in rich B medium (10 g/l bactopeptone, 1 g/l yeast extract and 1 g/l casaminoacids) using gentamicin (10 µg/ml) for selection.

Plant material and inoculation conditions

Tomato (*Solanum lycopersicum*) cultivars used were the susceptible cv. Marmande and the tolerant cv. Hawaii 7996. All plants were grown underlong-day light conditions and a light intensity of 120-150 µmol·m-2·s-1, at 25-26ºC and 60% relative humidity.

For bacterial inoculation in the apoplast, three- to four-week-old tomato plants were first acclimatized by transferring them to a chamber at 28 ºC with constant light conditions (12h light, 12h darkness). Two days later, plants were vacuum-infiltrated submerging the whole aerial part either in distilled water (mock) or in a 10^5 CFU/ml (OD_{600}=0.0001) suspension of the pathogen for approximately 20 seconds. In both cases, the adjuvant Silwet L-77 was added (80 µl/l suspension) to facilitate infiltration. After inoculation, plants were kept in the same conditions. Disease symptoms were evaluated using a scale measuring the affected surface of leaflets. Four levels of necrosis were defined: no necrosis (0% of affected surface), mild (< 25%), moderate (25-75%), and severe (> 75%). Leaflets from the third, fourth and fifth leaves of 24 plants per variety were evaluated.

Apoplastic fluid isolation

Apoplastic fluid isolation was performed following the protocol from Rico & Preston (38) and our previous experience (39). Briefly, tomato leaves were cut and vacuum-infiltrated with ice-cold distilled water. Infiltrated leaves were then blotted on a paper towel, rolled, and introduced into 5 ml tips (three-to-four leaves per tip), which were placed in 50 ml conical tubes (Falcon) containing 1.5 ml collection tubes (Eppendorf). Apoplast extract was collected by spinning the tubes at 3000 rpm for 15 min at 4ºC. For protein characterization, the supernatant was collected in new tubes, passed through a 0.22µm filter to get rid of any bacteria, and stored at -80ºC.

In planta bacterial growth quantification

Bacterial growth was measured by plating ten-fold dilutions of apoplastic fluid from infiltrated leaves on B medium plates, which were then incubated at 28ºC for 1-2 days. Colony Forming Units (CFUs) were counted and bacterial growth was calculated as CFUs/ml of collected apoplastic fluid.

Labelling reactions and inhibition assays

Equal volumes of apoplastic fluid were labelled using specific activity-based probes to detect papain-like cysteine protease (PLCP) and serine hydrolase (SH). All labelling reactions were performed at room temperature in dark conditions in a final volume of 50 µl. For fluorescent PLCP labelling, plant extracts were incubated for 4h with 2 µM of the MV201 probe (40) in 50 mM sodium acetate (NaAc) pH 5, and 1 mM dithiothreitol (DTT). Fluorescent SH labelling was performed incubating for 1h plant extracts with 2 µM of a fluorophosphonate (FP)-based probe (41) in 50 mM NaAc pH 5. Labelling was stopped by adding gel loading buffer to the samples and boiling at 95ºC for 5 min before electrophoresis.

Inhibition assays were performed by pre-incubating apoplastic fluids with specific inhibitors for 30 min previous to enzyme labelling. PLCPs were inhibited by 100 µM E-64 protease inhibitor, whereas a 200 µM cocktail composed of diisopropyl fluorophosphate (DFP), 3,4-dichloroisocoumarin (DCI), and phenylmethylsulfonyl fluoride (PMSF) was used to inhibit SHs.

Protein samples were separated on 10% sodium dodecylsulfate-polyacrylamide gel electrophoresis (SDS-PAGE) gels. Fluorescently labeled proteins were detected by fluorescence on the gel using a Typhoon 9400 scanner (Amershan Biosciences) and fluorescence intensity was measured using the ImageQuant TL software (GE Healthcare Life Sciences). Gels were then fixed by two 15 min incubation in a 50% methanol 7% acetic acid solution. After fixation, proteins were stained overnight with SYPRO® Ruby (Invitrogen) following the manufacturer's instructions. Finally, gels were rinsed under agitation with washing solution (10% methanol, 7% acetic acid) for 30 min. Fluorescent-stained gels were scanned using the Fujifilm LAS4000 image system. During staining and the subsequent steps, the gel was protected from light.

Affinity protein purification and in-solution protein digestion

Large-scale labelling was performed using biotinylated versions of the PLCP and SH activity probes, namely DCG-04 (42, 43) and FP-biotin (41) (Santa Cruz Biotechnology). Both probes were mixed together in a 4 ml labelling reaction mixture (50 mM NaAc pH 5, 5 mM DTT, 4 µM of each probe) and incubated for 4h. Proteins were then precipitated using the methanol-chloroform method. Briefly, 4 volumes (*v*) of cold methanol, 1 *v* of chloroform, and 3 *v* of cold MilliQ water were added to each sample, vortexing between every addition step. Samples were centrifuged at 3000 *g* for 45 min and the aqueous layer was removed. Then 4 *v* of methanol were added to each sample and centrifuged again at 3000 *g* for 45 min.

The liquid phase was discarded and the pellet dried at room temperature. Then 2 ml of 1.2% SDS-PBS was added and the pellet was dissolved completely by pipetting. Proteins were denatured by incubating the samples at 90ºC in a water bath for 5 min, and then 12 ml 1x PBS were added to lower the SDS concentration to less than 0.2%. Avidin beads (Sigma Aldrich) were incubated with each sample for 1h under rotation and then collected by spinning down at 400 *g* for 10 min. The supernatant was removed and the beads washed three times with 1.2% SDS-PBS, then with 1%SDS-PBS, then with 1x PBS, and finally with MilliQ water. The beads and remaining water were then transferred into 1.5 ml low binding protein tubes and spun down 400 *g* for 10 min to remove the remaining liquid. Finally, on-bead trypsin digestion was performed as described by Weerapana & collaborators (44). Tryptic samples were stored at -20ºC.

In-solution digestion of protein samples was performed following the protocol by Kessler Lab-Proteomics (http://www.tdi.ox.ac.uk/protocols-and-tools). Briefly, proteins were reduced with 5 mM DTT for 45 min, alkylated with 20 mM iodoacetamide for 45 min, and then precipitated via methanol-chloroform. The protein pellet was re-suspended in 6 M urea-Tris buffer, pH 7.8, and sonicated. Finally, urea concentration was brought to less than 1 M with MilliQ water and proteins were digested with trypsin (incubation O/N at 37ºC). Tryptic samples were stored at -20ºC. Prior to mass spectrometry analysis, all peptide samples were purified using SEP-PAK C18 columns (Waters) previously equilibrated with a solution of 65% acetonitrile (ACN) and 0.1% formic acid (FA) in Milli-Q water. The peptide digest samples were then added into a 2% ACN and 0.1% FA solution to the column, washed with this same solution, and eluted with 65% ACN and 0.1% FA. Finally, purified peptides were dried down completely in a speed-vac, resuspended in 20 µl of 2% ACN and 0.1% FA, and stored at -20ºC.

In total, three biological replicates were analyzed for each experimental condition (intersection of tomato variety and treatment) in both the pull-down and in-solution approaches.

LC-MS/MS

Experiments were performed on an Orbitrap Elite instrument (Thermo) (45) coupled to an EASY-nLC 1000 liquid chromatography (LC) system (Thermo) operated in the one-column mode. The analytical column was a fused silica capillary (75 µm × 27 cm) with an integrated PicoFrit emitter (New Objective) packed in-house with Reprosil-Pur 120 C18-AQ 1.9 µm resin (Dr. Maisch). The analytical column was encased by a column oven (Sonation) and attached to a nanospray flex ion source (Thermo). The column oven temperature was adjusted to 45 °C during data acquisition and at 30 °C in all other modes. The LC was equipped with two mobile phases: solvent A (0.1% formic acid, FA, in water) and solvent B (0.1% FA in acetonitrile, ACN). All solvents were of UPLC grade (Sigma). Peptides were directly loaded onto the analytical column with a flow rate of approximately 0.5 – 0.8 µL/min, which did not exceed 980 bar. Peptides were subsequently separated on the analytical column by running a 140 min gradient of solvent A and solvent B (start with 7% B; gradient 7% to 35% B for 120 min; gradient 35% to 100% B for 10 min and 100% B for 10 min) at a flow rate of 300 nl/min. The mass spectrometer was set in the positive ion mode and operated using Xcalibur software (version 2.2 SP1.48). Precursor ion scanning was performed in the Orbitrap analyzer (FTMS; Fourier Transform Mass Spectrometry) in the scan range of m/z 300-1800 and at a resolution of 60000 with the internal lock mass option turned on (lock mass was 445.120025 m/z, polysiloxane) (46). Product ion spectra were recorded in a data-dependent fashion in the ion trap (ITMS) in a variable scan range and at a rapid scan rate. The ionization potential was set to 1.8 kV. Peptides were analyzed using a repeating cycle consisting of a full precursor

ion scan (1.0 × 106 ions or 50 ms) followed by 15 product ion scans (1.0 × 104 ions or 100 ms) where peptides are isolated based on their intensity in the full survey scan (threshold of 500 counts) for tandem mass spectrum (MS2) generation that permits peptide sequencing and identification. Collision induced dissociation (CID) energy was set to 35% for the generation of MS2 spectra. During MS2 data acquisition dynamic ion exclusion was set to 60 seconds with a maximum list of excluded ions consisting of 500 members and a repeat count of one. Ion injection time prediction, preview mode for the FTMS, monoisotopic precursor selection and charge state screening were enabled. Only charge states higher than 1 were considered for fragmentation.

Peptide and Protein Identification using MaxQuant

RAW spectra were submitted to an Andromeda (47) search in MaxQuant (version 1.5.3.30) using the default settings (48). Label-free quantification and match-between-runs was activated (49). MS/MS spectra data were searched against the Uniprot *Ralstonia solanacearum* (UP000001436_267608.fasta; 5001 entries, downloaded 5/31/2017) and *Solanum lycopersicum* (UP000004994_4081.fasta; 33952 entries, downloaded 5/31/2017) databases. To estimate the level of contamination, all searches included a contaminants database (as implemented in MaxQuant, 245 sequences) that contains known MS contaminants. Andromeda searches allowed oxidation of methionine residues (16 Da) and acetylation of the protein N-terminus (42 Da) as dynamic modifications and the static modification of cysteine (57 Da, alkylation with iodoacetamide). Digestion mode was set to "specific", Enzyme specificity was set to "Trypsin/P" with 2 missed cleavages allowed, the instrument type in Andromeda searches was set to Orbitrap and the precursor mass tolerance to ±20 ppm (first search) and ±4.5 ppm (main search). The MS/MS match tolerance was set to ±0.5 Da and the peptide spectrum match FDR and the protein FDR to 0.01 (based on

target-decoy approach and decoy mode "revert"). Minimum peptide length was 7 amino acids. Minimum score for unmodified peptides was set to 0. All peptide relevant evidence data can be found in supplemental Table S1. For protein quantification modified peptides (minimum score 40) and unique and razor peptides were allowed. Further analysis and annotation of identified peptides was done in Perseus v1.5.5.3 (50). Processed data can be found in supplemental Tables S2 and S3. Only protein groups with at least two identified unique peptides over all runs were considered for further analysis. For quantification we combined related biological replicates to categorical groups and investigated only those proteins that were found in at least one categorical group in a minimum of 2 out of 3 biological replicas. Comparison of protein group quantities (relative quantification) between different MS runs is based solely on the LFQ's as calculated by MaxQuant (MaxLFQ algorithm). Briefly, Label-free protein quantification was switched on, and unique and razor peptides were considered for quantification with a minimum ratio count of 2. Retention times were recalibrated based on the built-in nonlinear time-rescaling algorithm. MS/MS identifications were transferred between LC-MS/MS runs with the "Match between runs" option in which the maximal match time window was set to 0.7 min and the alignment time window set to 20 min. The quantification is based on the "value at maximum" of the extracted ion current. At least two quantitation events were required for a quantifiable protein (46).

Experimental design and statistical rationale

For disease evaluation (see *Plant material and inoculation conditions*) a total of 24 plants per variety were used, and the leaflets from the third, fourth and fifth leaves were evaluated. Bacterial growth was quantified collecting the apoplast from four independent leaflets of three different plants. The mean of CFUs/ml and standard errors were calculated using these

three biological replicates. The experiment was repeated three times, all of them showing similar results.

For the activity-based and in-solution proteomic analyses (see *Affinity protein purification and in-solution protein digestion)* a total of three biological replicates were analyzed for each experimental condition. Each biological replicate was obtained pooling together apoplastic fluids obtained in three independent experiments in order to get the required apoplastic fluid amounts (4 ml). Twelve plants per condition were infiltrated in every experiment and distilled water was used as the mock-inoculation control.

Following peptide identification by LC/MS and processing using MaxQuant, and to provide robustness to the statistical analysis, non-valid detections were filtered out according to the following criteria: (i) for each experimental condition, detections missed in 2 out of the 3 replicates were not considered robust and therefore were replaced by *NaN* (*Not a Number*), and (ii), after (i), proteins missing (*NaN*) for all conditions were removed. To detect significant differences between conditions, we used the empirical Bayes method proposed by Kammers & collaborators (51), a moderated t-test that shrinks sample variances used in the estimation of the standard error of the observed fold changes (FC) towards a common mean. Consequently, statistical significance increases for proteins exhibiting large FC and relatively large sample variances (affecting the false negative rate) and decreases for proteins with small FC and relatively small sample variances (affecting the false positive rate). Variance shrinkage is sample size-dependent, diminishing with sample number. We used this model because it takes into account small sample sizes (in our case, three replicates) and missing data (*NaN* detections), two factors that influence variance. The test generated a statistic – called B-value– that summarizes the effect of both fold change and adjusted p-value for each protein: the higher the B-value, the higher the significance. The results of the test are summarized in supplemental Table S4.

Network construction

To analyze the interactome resulting from the analysis, we first uploaded the proteins detected in the in-solution experiments to STRING (v. 10.0). We generated a network for each experimental condition and used the information available from STRING regarding experimental evidence, databases, and coexpression analysis to establish putative interactions (edges). We uploaded the resulting networks to Cytoscape (v. 3.4.0) and clustered the nodes using the Community cluster (GLay) algorithm from clusterMaker assuming undirectionality of edges. To improve visualization, we bundled all the edges (number of handles: 3; spring constant: 0.003; compatibility threshold: 0.3; maximum iterations: 1000) and added the corresponding protein annotations from STRING databases.

Results

The tomato cultivar Hawaii 7996 survives leaf necrosis caused by R. solanacearum

To analyze the active proteome of the apoplast of the tolerant tomato Hawaii 7996 and compare it with that of the susceptible Marmande, we first needed a condition in which the bacterial populations present in both cultivars were comparable. Root inoculation methods usually lead to high variability in plant colonization due to stochasticity of the initial infection (52). Besides, protocols for the collection of large amounts of apoplastic fluid from the roots are yet to be optimized. To overcome these two limitations, and considering that *R. solanacearum* moves through an apoplastic environment during the first stage of the infection, we used leaf apoplast to study the intercellular plant proteome triggered in response to the pathogen.

To set up the inoculation system, we vacuum-infiltrated the aerial part of Marmande (susceptible cultivar) and Hawaii 7996 (tolerant cultivar) tomato plants with 10^5 CFU/ml bacteria and monitored symptoms over time. Vacuum-infiltration of leaves ensured equal pathogen inocula among replicates. *R. solanacearum* growth caused tissue necrosis in both cultivars, although the magnitude of the lesions was much lower in Hawaii 7996 (Fig. 1*A*). Necrotic lesions were evaluated over time using a semi-quantitative scale (Fig. 1*B*). Tissue necrosis appeared 2 days post-inoculation (dpi), and became more severe by 3 dpi. Interestingly, leaflet necrosis developed quicker in Marmande compared to Hawaii 7996, and at 8 dpi the susceptible cultivar was completely dead. To test if differential leaf necrosis was explained by the extent of bacterial multiplication in planta, we collected apoplastic fluid of inoculated leaves at 0 to 8 dpi and quantified bacterial growth. Surprisingly, we did not detect any growth difference between the apoplasts of Marmande and Hawaii 7996 at early time points (Fig. 1*C*), suggesting that Hawaii 7996 behaves as tolerant when the pathogen is infiltrated in the leaves. However, bacterial loads decreased drastically only in Marmande plants when advanced tissue necrosis was apparent at later stages of the infection, as expected. Although the bacterial multiplication did not correlate with the decreased leaf necrosis observed in Hawaii 7996, the protein content in the infected apoplast of this variety was higher than that of Marmande (Fig. S1*A*), and some proteins were specifically induced in the apoplast of the tolerant cultivar upon infection (Fig. S1*B*). These data support the notion that molecular mechanisms related to activation of certain proteins may underpin defense in tolerant cultivars.

Apoplastic PLCP and SH activities are induced in response to R. solanacearum infection

We then tested if the proteins induced in the apoplast of Hawaii 7996 (Fig. S1*B*) belonged to the PLCP or the SH families of proteases using ABPP (Fig. S2*A*). To monitor PLCP and SH activities, apoplastic fluid from mock- and *R. solanacearum*-infiltrated Marmande and Hawaii 7996 leaves was collected at 2 dpi. At this stage, intercellular spaces were readily colonized by comparable amounts of the pathogen in both varieties and the absence of necrosis ensured low cytoplasmic contamination, which was confirmed when blotting apoplastic and total protein extracts against the cytosolic protein ascorbate peroxidase (cAPX) (Fig. S3). Apoplastic fluids from three independent experiments were labelled using two distinct activity-based probes (Fig. S4): MV201, a fluorescent derivative of E-64 which specifically labels PLCPs (40), and a fluorophosphonate (FP)-based probe that reacts with the conserved serine active site nucleophile of SHs (41). Labelling with MV201 showed one major signal above 25 kDa on both tomato cultivars (Fig. 2*A*, *first panel*). Importantly, the quantification of this activity from three independent experiments was significantly stronger in infected Hawaii 7996 (Fig. 2*B*, *first graph;* Fig S6A, *first panel*). The signal was largely inhibited when we pre-incubated the apoplastic fluid with the PLCP inhibitor E-64, further confirming the predicted activity (Fig. 2*C*, *first panel*). On the other hand, the FP probe detected two SH signals above the 70 and the 55 kDa reference proteins (Fig. 2*A, second panel*). Both bands were significantly more induced in infected Hawaii 7996 (Fig. 2*B*, *second and third graph;* Fig S6A*, second panel*). Both bands were partially inhibited by a cocktail of SH inhibitors composed of diisopropyl fluorophosphate (DFP), 3,4-dichloroisocoumarin (DCI), and phenylmethylsulfonyl fluoride (PMSF), confirming the predicted activities (Fig. 2*C*, *second panel*). Additionally, most of the PLCP and SH signals –except for the 55 kDa SH– were not detected at earlier stages of the infection (Fig. S5 and S6B), suggesting a delayed and/or challenge-dependent activation of these proteases. The differential increase in PLCP and SH extracellular activities between Marmande and Hawaii 7996 was indicative of

a specific protein activity signature against *R. solanacearum* in the tolerant tomato cultivar, which could contribute to the observed limited necrosis in this variety.

Identification of differentially active PLCPs and SHs

To identify the enzymes responsible for the differential PLCP and SH activities and quantify their contribution to the response, we labelled the apoplastic fluids from three independent experiments with the DCG-04 and FP-biotin probes (Fig. S2*B*). DCG-04 is a biotinylated version of MV201 which specifically labels PLCPs (42, 43), while FP-biotin reacts with SHs (41). Labelled proteins were affinity-purified and identified by mass spectrometry, yielding a total of 335 protein groups. Protein detections were filtered using stringent confidence parameters: first, proteins detected only once per experimental condition –missed in 2 out of the 3 biological replicates– were not considered robust and the corresponding detection value was omitted; second, and after applying the first filter, we removed those proteins for which detections were missing in all conditions. After filtering out non-robust detections 175 proteins remained. Of those, 11 classified as PLCPs according to their PFAM annotation, and 69 showed serine-type hydrolase activity. Significant changes in active protein abundance were detected using a moderate t-statistic (described in the *Experimental procedures* section). The results of the test are summarized in supplemental Table S4. Using this model we detected 4 differentially active PLCPs and 27 SHs (Fig. 3). These activities correlated with the 25, 55 and >70 kDa bands detected in protein gels using fluorescently labelled probes (Fig. 2). Among these 31 differentially activated proteases, 25 were predicted to contain a signal peptide, according to the existent annotations in the UniProtKB and PFAM databases and the domain prediction software DeepLoc-1 (53). Further, 23 out of the 31 differentially activated proteins were predicted as extracellular. Only 8 were predicted as not extracellular and, among these, 2 have been shown to localize and function in the apoplast (54).

Out of the four identified PLCPs, only the peptidases Rcr3 and Pip1 (*Phytophthora* inhibited protease 1) showed >2-fold intensity changes (Fig. 3*A*-*D*). Rcr3 and Pip1 activity was induced upon infection in susceptible plants, but only the activity of Pip1 was significantly induced in Hawaii 7996 (Fig. 3*C* and *D*). Interestingly, the levels of active Rcr3 were constitutively active in the tolerant cultivar (about 4-fold the amount in susceptible Marmande; Fig. 3*A*), and did not change significantly when infected by *R. solanacearum* (Fig. 3*D*). In addition, two unannotated PLCPs (Solyc01g110110.2.1 and Solyc07g041920.2.1) were also significantly affected by *R. solanacearum* infection, showing slightly reduced activity levels in the tolerant plant (Fig. 3*E*).

Several active SHs from six main protease classes changed significantly upon infection. In particular, 11 SHs had S8 subtilisin-like protease activity (S8 SLP), 4 were identified as S10 serine carboxypeptidases (S10 SCP), 7 belonged to the GDSL-like lipase superfamily, 2 presented a class 3 lipase domain, 2 an α/β hydrolase 3 domain, and 1 had pectinacetylesterase activity (Fig. 3). The P69 SLP family was well represented in the analysis, with the activity of P69B, P69C and P69F highly induced in infected plants. While the induction of active P69B was detected both in Marmande and Hawaii 7996 plants, the levels of active P69C were almost 2-fold lower in Hawaii 7996. Interestingly, the activity of P69F was one of the two most induced (up to 5-fold) SHs in Hawaii 7996, whereas it was not detected in Marmande (Fig. 3*C* and *D;* Table S2). Additionally, two unannotated SHs, the SLP Solyc08g079900.1.1 and the SCP Solyc05g041540.2.1 showed a strong activity induction (5- and 2-to-3-fold changes, respectively) in infected plants (Fig. 3*E*). Importantly, members of the α/β hydrolase and GDSL-like lipase superfamilies also experienced significant changes in activity. The two identified α/β hydrolase 3 were only detected upon infection, and the activity of the class 3 lipase Solyc02g077110.2.1 was highly induced upon infection exclusively in Marmande. Interestingly, the activity of all 7 GDSL-like lipases was

downregulated in the presence of *R. solanacearum,* especially in Hawaii 7996 plants. Four of them, including Cutin-deficient 1 protein (CD1), remained slightly higher in infected Marmande than Hawaii 7996.

P69C, P69F and Solyc02g077110.2.1 are post-translationally activated

To determine whether protein activity changes were linked to changes in abundance or were due to post-translational modifications, we performed an in-solution digest of all proteins present in the apoplast from the samples used for ABPP and analyzed them by mass spectrometry (Fig. S2*C*). Protein detections were filtered using the same criteria as before, from which 1145 proteins remained. A total of 144 proteins were shared by both datasets (pull-down and in-solution digest). We compared the detection intensities from the activity-based pull-down approach –hereafter referred as "activity"– to those obtained in the in-solution digest –referred as "abundance"–. Upon infection, some proteins were significantly more detected in the activity-based approach without experiencing a significant change in abundance, indicating post-translationally-driven protein activation rather than overexpression. To identify these proteins, we calculated the ratio between activity and abundance intensities for the 144 shared proteins and compared the effect of *R. solanacearum* infection in both varieties (Fig. 4*A*). Three proteins, the P69 family members P69C and P69F, and the unannotated Solyc02g077110.2.1 (K4B8T8) were specifically activated by *R. solanacearum*, as they showed a significant increase in the activity/abundance ratio upon infection (Fig. 4*B*). In the case of K4B8T8, abundance remained constant while activity increased and the high increase in activities of P69C and F after infection are accompanied by minor increases in their abundances (Fig. 4*B*). Since many of the genes that were activated or inactivated also suffered changes in protein abundance, we checked their expression levels upon *R. solanacearum* natural infection. Available gene expression data (55) showed that

gene expression correlated with protein abundance in our study (Fig. S7A). This data was validated in our own experimental conditions for 3 selected genes (Fig. S7B).

On the other hand, some proteins were not detected in one of the two treatments (they were present in mock-inoculated samples but not in *R. solanacearum*-infected ones, or the opposite) (Fig. S8). Although activity changes could not be measured for these proteins, they may still represent good candidates for proteins potentially inhibited or activated in the apoplast upon challenge with *R. solanacearum*. Interestingly, and consistent with our previous analysis (Fig. 3), three GDSL-like lipases were identified as potentially inhibited proteins, while five α/β hydrolases 3 and 6 were activated in the presence of *R. solanacearum*.

The context-specific protein networks driving the tomato response to R. solanacearum infection are variety-dependent

To understand how *R. solanacearum* infection affects the apoplastic interactome of the two varieties, we generated 4 interaction networks, *i.e.* one for each experimental condition (Fig. 5). Each network captured the molecular mechanisms in which the proteins detected in the in-solution experiment are involved according to literature. Specifically, we compiled all protein-protein interactions among detected proteins, as well as those between a detected protein and an undetected one. Only curated interactions were included, as described in the *Experimental Procedures* section. Each protein was represented by a network node, and interactions were represented as edges. The resulting networks were composed of 593-606 nodes and 4165-4499 edges (depending on the condition). To further characterize the interactome that drives the apoplastic response in each condition/variety combination, node size was adjusted to detection intensity and functional and stress-related annotations were added in order to visualize the putative changes caused by *R. solanacearum*. This yielded four highly context-specific, mechanistic models of infection response. Within the networks,

we highlighted protein families that could be directly or indirectly related with defense responses. Peroxidases and glycosidases, for instance, have been shown to participate in cell wall remodeling processes, a strategy that could be used by plants to fight pathogen infection (56, 57). Community-based clustering revealed that peroxidases and glycosidases, as well as oxidative stress-related proteins formed known clusters, hence highlighting the non-randomness of the interactome.

Network comparison indicated that, in general terms, the pathways involved in the infection response of Marmande experienced more topological changes than in Hawaii 7996 (Fig. 5). For example, peroxidases increased their promiscuity with other proteins in the presence of *R. solanacearum* only in Marmande, where they recruit other proteins related to oxidative stress; and the opposite situation could be observed for glycosidases (Fig. 5*A* and *B*). In Hawaii 7996, both peroxidases and glycosidases clustered separately, isolated from other functions (Fig. 5*C* and *D*), therefore suggesting no major functional changes upon infection.

Interestingly, one protein with LRR (Leucine-Rich Repeat) domain (Solyc04g074000.2.1) appeared only after infection (Fig. 5*B* and *D*), being undetectable in mock conditions of both varieties. Upon infection this LRR protein clustered together with other proteins that participate in plant-pathogen interaction responses. On the other hand, the only subtilase (Solyc03g025610) that exhibits a connection was clustered near these biotic stress-related modules (Fig. 5*B*-*D*).

Discussion

Tomato apoplast to study the molecular basis of resistance to R. solanacearum

Plant resistance against *R. solanacearum* is multilayered, combining structural, chemical and molecular defense mechanisms that are far from being elucidated. In tomato, no resistance gene has been identified and quantitative traits explain only a portion of resistance against *R. solanacearum* (21, 24, 25, 27). The apoplast is known as one of the major battlegrounds of plant-pathogen interactions. Its slightly acidic pH makes it ideal for selective activation of secreted proteases that act against the invading pathogen (58). To reach the xylem, *R. solanacearum* preferentially moves intercellularly using the apoplastic route (22, 59, 60). Plant proteases specifically activated against pathogens are rapid and powerful weapons to stop infection (29). The goal of this study was to identify and characterize the tomato apoplastic protease activities triggered by *R. solanacearum* infection in tolerant and susceptible tomato cultivars. For this, we performed activity-based protein profiling, a state of the art technique to discover active protein landscapes (61), from infected and uninfected tomato apoplasts.

Equal loads of *R. solanacearum* caused markedly different symptoms in the tolerant tomato variety Hawaii 7996 compared to the susceptible Marmande (Fig. 1*A* and *B*). Although necrosis was observed in both varieties early after infection (2 dpi), Hawaii 7996 plants stayed turgid, whereas Marmande plants wilted. Unexpectedly, apoplastic bacterial growth remained comparable in both varieties before Marmande started wilting (Fig. 1*C*). This observation indicated that Hawaii 7996 apoplastic defense mechanisms do not target bacterial growth, but may rather limit its pathogenic behavior. This notion was supported by the fact that at 2 dpi the apoplastic protein abundance in Hawaii 7996 was higher and contained an induced protein diversity not apparent in Marmande. Increased apoplastic activities have been reported upon treatment with benzothiadiazole (BTH), an analog of the plant hormone salicylic acid that is involved in induced broad-spectrum disease resistance responses (58, 62).

Plant responses to R. solanacearum involve differential activation of apoplastic PLCPs and SHs

ABPP allowed us to determine variety- and infection-specific changes in protein activity. Using probes to detect the activities of PLCPs and SHs, proteases with the best understood function in the plant-pathogen context (32), we found a specific overactivation of SHs in tolerant Hawaii 7966 plants challenged with *R. solanacearum*, compared to the susceptible variety Marmande (55 and 70 kDa bands in Fig. 2*A* and *B*). This differential SH activity induction correlates with the previously mentioned increased protein loads detected in the tolerant cultivar (Fig. S1). PLCPs were activated in response to infection in both the susceptible and tolerant cultivars, but activation was significantly more pronounced in the latter (Fig. 2*A* and *B*).

Identification of proteases potentially associated with the described differential protein activities was achieved using immunoaffinity purification linked to mass-spectrometry of apoplastic fluids of infected or non-infected Marmande and Hawaii 7996. This high-throughput analysis yielded several potentially interesting candidates. Among the differentially activated SHs, the uncharacterized P69 family member P69F was one of the two most activated (up to 5-fold) in Hawaii 7996 (Fig. 3D), whereas it was not detected in Marmande (Fig. 3*C* and *E*). This might reveal an important role for this protease in the molecular defense of the tolerant cultivar against *R. solanacearum*. Unlike P69F, the tomato P69 family members P69B and P69C were suggested to respond to the defense hormone salicylic acid and *Pseudomonas syringae* effectors in *A. thaliana* (63, 64). P69B was previously identified as transcriptionally upregulated in potato challenged with *R. solanacearum* (65), *P. infestans* (62) and the citrus exocortis viroid (66), and is also targeted by the protease inhibitors EPI1 and EPI10 secreted by *P. infestans* (62, 67). It will be

interesting to elucidate the specific role in defense of P69F and whether its pathogen-inducible activity linked to defense is conserved among different plant pathosystems.

The activity pull-down experiment revealed 4 differentially activated PLCPs. Among them, two known defense-induced PLCPs, Rcr3 and Pip1, displayed strong activation upon infection. The statistical analysis showed an enhanced induction of both Rcr3 and Pip1 in Marmande plants while only Pip1 was overactivated in infected Hawaii 7996 (Fig. 3*E*), contrasting with the bands obtained in protein gels (Fig. 2*A* and *B*). This disparity might be explained by a minor but potentially synergistic effect of other PLCPs, which could contribute to the band intensity in Hawaii 7996 without being revealed as significant in the applied test. Pip1 was previously reported as a broad-range contributor of the tomato defense against fungal, bacterial, and oomycete apoplastic pathogens (54), while Rcr3 depletion increased susceptibility to the oomycete *P. infestans* (68, 69), the leaf mold *C. fulvum* (35, 70), and the potato cyst nematode *Globodera rostochiensis* (36). Our data may suggest a different mode of action of these two proteases: Pip1 was overactivated both in Marmande and Hawaii 7996, while Rcr3 already showed high basal levels in Hawaii 7996 mock-inoculated plants, implying that it might not need further activation to favor plant defense.

Both Pip1 and P69B were found to be transcriptionally upregulated in the stems of the tolerant cultivar LS-89 inoculated with *R. solanacearum* (71). Additionally, Pip1 was upregulated in 5 other tolerant cultivars, including Hawaii 7996, and did not change significantly in susceptible tomato varieties (71). In contrast, Pip1 transcription increased in the leaves of both susceptible and tolerant tomato challenged with the apoplastic pathogens *Cladosporium fulvum* and *Pseudomonas syringae*, and quantitative proteomic analysis detected Pip1 protein in leaf apoplasts (54). Similar results were observed for Rcr3. Our results coincide with these latter findings, since an increase in Pip1 activity was also detected in the apoplast of the *R. solanacearum*-susceptible and tolerant tomato cultivars. Overall, our

findings add new insights to the broad-range immunity role of Pip1 in the leaf apoplast, and which might also have a role at the root interface (Fig. S7).

Comparison of differential protein activation to protein abundance in the different samples revealed that P69F and P69C showed a significant and robust increase in their activity/abundance ratio after infection. This finding indicates that these two proteins may be subjected to post-translational modifications for activation. Besides P69C and F, an unannotated protein, Solyc02g077110.2.1 (K4B8T8), showed a significantly high activity/abundance ratio. This protein is predicted to have a class 3 lipase domain with a serine in its active site, and to participate in lipid metabolic processes. Lipases have been previously detected using SH activity probes due to the presence of a catalytic serine residue in their active site (37). Our findings suggest that Solyc02g0771102.1 is specifically activated in response to *R. solanacearum* infection. Further analysis of these lipases will help determine whether they act as SHs, their mode of action and their substrates at the plant-pathogen interphase, expanding our knowledge on plant defense mechanisms.

In our analysis, we detected a generalized inactivation of GDSL-like lipases upon infection. GDSLs comprise an extremely broad gene family with more than 1100 members found in the 12 fully sequenced plant genomes (72). Most have no function assigned yet and amongst many different processes, some lipases have been shown to participate in defense against several plant pathogens. In *A. thaliana*, the activity of GDSL-like lipases was detected by FP-labelling upon *Botrytis cinerea* infection (37). In addition, the secreted GDSL lipase GLIP1 contributed to defense against necrotrophic fungi and negatively regulated defense against (hemi)biotrophic pathogens. Recombinant AtGLIP1 showed antimicrobial activity against fungal spores, inhibiting their germination and severely altering their morphology, suggesting a role in the disruption of the fungal cell wall and/or membrane (73). AtGLIP1 also triggered systemic resistance when the plants were challenged with the necrotrophic fungus *Alternaria*

brassicicola, requiring ethylene signaling (73, 74). *A. thaliana glip1* mutants showed enhanced susceptibility to *Alternaria brassicicola*, the bacterial necrotroph *Erwinia carotovora* and the hemibiotroph *Pseudomonas syringae* pv. *tomato*, while its overexpression increased resistance (74). Likewise, AtGLIP2 has also been shown to participate in defense against necrotrophs, since *glip2* mutants were more susceptible to *Erwinia carotovora* (75). In contrast, pepper CaGLIP1 overexpression caused enhanced susceptibility against the biotrophic oomycete *Hyaloperonospora parasitica* and *Pseudomonas syringae* pv. *tomato* (76). Although the role that GDSL lipases have in the defense against *R. solanacearum* is yet to be elucidated, their global inactivation in Hawaii 7996 –as detected in our analysis– might indicate that they constitute susceptibility genes, whose action needs to be inhibited in order to enhance resistance.

In summary, we propose that the P69 family proteases and the PLCPs Rcr3 and Pip1 play a role in apoplastic defense against *R. solanacearum* as has been shown for other plant pathogens. We suggest that these identified proteases are important to block some bacterial activities that may not be relevant for multiplication in the apoplast but that may be key for the next steps (i.e bacterial colonization of the xylem vessels). Finally, our screen revealed several other unannotated/uncharacterized PLCP and SH activities, opening new avenues for molecular dissection of the apoplastic protease landscape induced by infection.

Protein network analysis reveals topological changes in response to infection

Our network analysis revealed that the mechanisms/pathways involved in the response to infection by *R. solanacearum* of susceptible Marmande experience more topology changes than that of tolerant Hawaii 7996. The deeper readjustment of the Marmande protein networks in response to infection manifests primarily as different nodes increase promiscuity, recruiting other nodes related to stress responses. This is the case of glycosylases and

peroxidases. This massive reorganization of the protein network related to stress probably results from the combination of both unsuccessful activation of plant defense responses and damage caused by the pathogen. In contrast the protein networks in the tolerant tomato variety Hawaii 7996 undergo fewer adjustments due to infection. This could suggest that the tolerant variety may be more prepared to respond to stress situation in its basal condition.

Although the vast majority of proteins identified in the ABPP pull-down experiment involved in the response against the pathogen could not be plotted due to lack of interactions, network analysis revealed an unannotated LRR-containing protein that appeared specifically after infection. This protein clustered together with other LRR proteins predicted to participate in defense responses, which could indicate an important role of this pathogen receptor protein in response to *R. solanacearum* infection.

Data availability

Mass spectrometry proteomics data have been deposited to the ProteomeXchange Consortium via the PRIDE (77) partner repository (https://www.ebi.ac.uk/pride/archive/) under identifier PXD005603. During review, data can be accessed via a reviewer account (**Username:** reviewer45748@ebi.ac.uk; **Password:** eTD8Rqb1).

Acknowledgements

The authors would like to thank all members of the "bacterial plant diseases and cell death" lab for helpful comments. This work was funded by projects AGL2013-46898-R to N.S.C. and M.V., and RyC 2014-16158 to N.S.C. (Spanish Ministry of Economy and Competitiveness, MINECO, Spain); EU-Marie Curie Actions (PIIF-331392); ERC starting

grant No. 258413 to M.K.; ERC Consolidator Grant 616449 'GreenProteases' to R.H. and EuroTransBio project 'PredicSeed' to J.P. We acknowledge financial support from the "Severo Ochoa Programme for Centres of Excellence in R&D" 2016-2019 (SEV-2015-0533) and the CERCA Programme / Generalitat de Catalunya, from DFG (grant No. INST 20876/127-1 FUGG to M.K.) and from COST Action SUSTAIN (FA1208).

Author contribution

MP performed and designed experiments, analyzed data and wrote the manuscript

MB analyzed data and assisted in manuscript writing

JP performed experiments and analyzed data

FK performed the mass spectrometry (MS) experiments and performed the initial MS data analysis

MK performed the mass spectrometry (MS) experiments and performed the initial MS data analysis

MV designed the research, analyzed data and wrote the manuscript

RAL designed the research, analyzed data and assisted in manuscript writing

NSC designed the research, analyzed data and wrote the manuscript

All authors reviewed the manuscript

References

1. Mansfield, J., Genin, S., Magori, S., Citovsky, V., Sriariyanum, M., Ronald, P., Dow, M., Verdier, V., Beer, S. V., Machado, M. A., Toth, I., Salmond, G., and Foster, G. D.

(2012) Top 10 plant pathogenic bacteria in molecular plant pathology. *Mol. Plant Pathol.* 13, 614–629

2. Hayward, A. (1991) Bacterial Wilt Caused By Pseudomonas solanacearum. *J. Plant Pathol.* 95, 237–245
3. Elphinstone, J. (2005) in *Bacterial wilt disease and the Ralstonia solanacearum species complex*, eds Allen C, Prior P, Hayward A (American Phytopathological Society, St. Paul), pp 9–28.
4. Genin, S. (2010) Molecular traits controlling host range and adaptation to plants in Ralstonia solanacearum. *New Phytol.* 187, 920–928
5. Grimault, V., and Prior, P. (1994) Grafting Tomato Cultivars Resistant or Susceptible to Bacterial Wilt - Analysis of Resistance Mechanisms. *J. Phytopathol.* 141, 330–334
6. Peregrine, W. T. H., and bin Ahmad, K. (1982) Grafting—A simple technique for overcoming bacterial wilt in tomato. *Trop. Pest Manag.* 28, 71–76
7. Rivard, C. L., O'Connell, S., Peet, M. M., and Louws, F. J. (2012) Grafting Tomato to Manage Bacterial Wilt Caused by Ralstonia solanacearum in the Southeastern United States. *Plant Dis.*, 973–978
8. Grimault, V., Anais, G., and Prior, P. (1994) Distribution of Pseudomonas solanacearum in the stem tissues of tomato plants with different levels of resistance to bacterial wilt. *Plant Pathotogy* 43, 663–668
9. Wang, J. F., Hanson, P., and Barnes, J. (1998) in *Bacterial Wilt Disease: Molecular and Ecological Aspects*, eds Prior P, Allen C, Elphinstone J (Springer, Berlin), pp 269–275.
10. Prior, P., Bart, S., Leclercq, S., Darrasse, a, and Anais, G. (1996) Resistance to bacterial wilt in tomato as discerned by spread of Pseudomonas (Burholderia) solanacearum in the stem tissues. *Plant Pathol.* 45, 720–726

11. Deslandes, L., Olivier, J., Peeters, N., Feng, D. X., Khounlotham, M., Boucher, C., Somssich, I., Genin, S., and Marco, Y. (2003) Physical interaction between RRS1-R, a protein conferring resistance to bacterial wilt, and PopP2, a type III effector targeted to the plant nucleus. *Proc. Natl. Acad. Sci. U. S. A.* 100, 8024–9

12. Narusaka, M., Shirasu, K., Noutoshi, Y., Kubo, Y., Shiraishi, T., Iwabuchi, M., and Narusaka, Y. (2009) RRS1 and RPS4 provide a dual Resistance-gene system against fungal and bacterial pathogens. *Plant J.* 60, 218–226

13. Le Roux, C., Huet, G., Jauneau, A., Camborde, L., Trémousaygue, D., Kraut, A., Zhou, B., Levaillant, M., Adachi, H., Yoshioka, H., Raffaele, S., Berthomé, R., Couté, Y., Parker, J. E., and Deslandes, L. (2015) A Receptor Pair with an Integrated Decoy Converts Pathogen Disabling of Transcription Factors to Immunity. *Cell* 161, 1074–1088

14. Sarris, P. F., Duxbury, Z., Huh, S. U., Ma, Y., Segonzac, C., Sklenar, J., Derbyshire, P., Cevik, V., Rallapalli, G., Saucet, S. B., Wirthmueller, L., Menke, F. L. H., Sohn, K. H., and Jones, J. D. G. (2015) A plant immune receptor detects pathogen effectors that target WRKY transcription factors. *Cell* 161, 1089–1100

15. Kim, B. S., French, E., Caldwell, D., Harrington, E. J., and Iyer-Pascuzzi, A. S. (2015) Bacterial wilt disease: Host resistance and pathogen virulence mechanisms. *Physiol. Mol. Plant Pathol.* 95, 37–43

16. Carmeille, A., Caranta, C., Dintinger, J., Prior, P., Luisetti, J., and Besse, P. (2006) Identification of QTLs for Ralstonia solanacearum race 3-phylotype II resistance in tomato. *Theor. Appl. Genet.* 113, 110–121

17. Mangin, B., Thoquet, P., Olivier, J., and Grimsley, N. H. (1999) Temporal and multiple quantitative trait loci analyses of resistance to bacterial wilt in tomato permit the resolution of linked loci. *Genetics* 151, 1165–1172

18. Thoquet, P., Olivier, J., Sperisen, C., Rogowsky, P., Laterrot, H., and Grimsley, N. (1996) Quantitative trait loci determining resistance to bacterial wilt in tomato cultivar Hawaii7996. *Mol. Plant. Microbe. Interact.* 9, 826–836

19. Thoquet, P., Olivier, J., Sperisen, C., Rogowsky, P., Prior, P., Anais, G., Mangin, B., Bazin, B., Nazer, R., and Grimsley, N. (1996) Polygenic resistance of tomato plants to bacterial wilt in the French West Indies. *Mol. Plant. Microbe. Interact.* 9, 837–842

20. Wang, J. F., Olivier, J., Thoquet, P., Mangin, B., Sauviac, L., and Grimsley, N. H. (2000) Resistance of tomato line Hawaii7996 to Ralstonia solanacearum Pss4 in Taiwan is controlled mainly by a major strain-specific locus. *Mol. Plant. Microbe. Interact.* 13, 6–13

21. Wang, J. F., Ho, F. I., Truong, H. T. H., Huang, S. M., Balatero, C. H., Dittapongpitch, V., and Hidayati, N. (2013) Identification of major QTLs associated with stable resistance of tomato cultivar "Hawaii 7996" to Ralstonia solanacearum. *Euphytica* 190, 241–252

22. Vasse, J., Frey, P., and Trigalet, A. (1995) Microscopic studies of intercellular infection and protoxylem invasion of tomato roots by Pseudomonas solanacearum. *Mol. Plant. Microbe. Interact.* 8, 241–251

23. Grimault, V., and Prior, P. (1993) Bacterial wilt resistance in tomato associated with tolerance of vascular tissues to Pseudomonas solanacearum. *Plant Pathol.* 42, 589–594

24. McGarvey, J. a, Denny, T. P., and Schell, M. a (1999) Spatial-Temporal and Quantitative Analysis of Growth and EPS I Production by Ralstonia solanacearum in Resistant and Susceptible Tomato Cultivars. *Phytopathology* 89, 1233–1239

25. Grimault, V., Gélie, B., Lemattre, M., Prior, P., and Schmit, J. (1994) Comparative histology of resistant and susceptible tomato cultivars infected by Pseudomonas solanacearum. *Physiol. Mol. Plant Pathol.* 44, 105–123

26. Nakaho, K., Hibino, H., and Miyagawa, H. (2000) Possible mechanisms limiting movement of Ralstonia solanacearum in resistant tomato tissues. *J. Phytopathol.* 148, 181–190

27. Nakaho, K., Inoue, H., Takayama, T., and Miyagawa, H. (2004) Distribution and multiplication of Ralstonia solanacearum in tomato plants with resistance derived from different origins. *J. Gen. Plant Pathol.* 70, 115–119

28. Gupta, R., Lee, S. E., Agrawal, G. K., Rakwal, R., Park, S., Wang, Y., and Kim, S. T. (2015) Understanding the plant-pathogen interactions in the context of proteomics-generated apoplastic proteins inventory. *Front. Plant Sci.* 6, 352

29. Jashni, M. K., Mehrabi, R., Collemare, J., Mesarich, C. H., and de Wit, P. J. G. M. (2015) The battle in the apoplast: further insights into the roles of proteases and their inhibitors in plant-pathogen interactions. *Front. Plant Sci.* 6, 584

30. Cravatt, B. F., and Sorensen, E. J. (2000) Chemical strategies for the global analysis of protein function. *Curr. Opin. Chem. Biol.* 4, 663–668

31. Verhelst, S. H. L., and Bogyo, M. (2005) Dissecting protein function using chemical proteomic methods. *QSAR Comb. Sci.* 24, 261–269

32. Kołodziejek, I., and van der Hoorn, R. A. L. (2010) Mining the active proteome in plant science and biotechnology. *Curr. Opin. Biotechnol.* 21, 225–233

33. Misas-Villamil, J. C., van der Hoorn, R. A. L., and Doehlemann, G. (2016) Papain-like cysteine proteases as hubs in plant immunity. *New Phytol.*,

34. Gilroy, E. M., Hein, I., Van Der Hoorn, R., Boevink, P. C., Venter, E., McLellan, H., Kaffarnik, F., Hrubikova, K., Shaw, J., Holeva, M., L??pez, E. C., Borras-Hidalgo, O., Pritchard, L., Loake, G. J., Lacomme, C., and Birch, P. R. J. (2007) Involvement of cathepsin B in the plant disease resistance hypersensitive response. *Plant J.* 52, 1–13

35. Krüger, J., Thomas, C. M., Golstein, C., Dixon, M. S., Smoker, M., Tang, S., Mulder,

L., and Jones, J. D. G. (2002) A Tomato Cysteine Protease Required for Cf-2-Dependent Disease Resistance and Suppression of Autonecrosis. *Science (80-.).* 296, 744–747

36. Lozano-Torres, J. L., Wilbers, R. H. P., Gawronski, P., Boshoven, J. C., Finkers-Tomczak, A., Cordewener, J. H. G., America, A. H. P., Overmars, H. A., Van 't Klooster, J. W., Baranowski, L., Sobczak, M., Ilyas, M., van der Hoorn, R. A. L., Schots, A., de Wit, P. J. G. M., Bakker, J., Goverse, A., and Smant, G. (2012) Dual disease resistance mediated by the immune receptor Cf-2 in tomato requires a common virulence target of a fungus and a nematode. *Proc. Natl. Acad. Sci. United States Am.* 109, 10119–24

37. Kaschani, F., Gu, C., Niessen, S., Hoover, H., Cravatt, B. F., and van der Hoorn, R. a L. (2009) Diversity of Serine Hydrolase Activities of Unchallenged and Botrytis-infected Arabidopsis thaliana. *Mol. Cell. Proteomics* 8, 1082–1093

38. Rico, A., and Preston, G. M. (2008) Pseudomonas syringae pv. tomato DC3000 uses constitutive and apoplast-induced nutrient assimilation pathways to catabolize nutrients that are abundant in the tomato apoplast. *Mol. Plant. Microbe. Interact.* 21, 269–282

39. Zuluaga, A. P., Puigvert, M., and Valls, M. (2013) Novel plant inputs influencing Ralstonia solanacearum during infection. *Front. Microbiol.* 4, 1–7

40. Richau, K. H., Kaschani, F., Verdoes, M., Pansuriya, T. C., Niessen, S., Stuber, K., Colby, T., Overkleeft, H. S., Bogyo, M., and Van der Hoorn, R. a. L. (2012) Subclassification and Biochemical Analysis of Plant Papain-Like Cysteine Proteases Displays Subfamily-Specific Characteristics. *Plant Physiol.* 158, 1583–1599

41. Liu, Y., Patricelli, M. P., and Cravatt, B. F. (1999) Activity-based protein profiling: The serine hydrolases. *Proc. Natl. Acad. Sci.* 96, 14694–14699

42. Greenbaum, D., Medzihradszky, K. F., Burlingame, A., and Bogyo, M. (2000) Epoxide electrophiles as activity-dependent cysteine protease profiling and discovery tools. *Chem. Biol.* 7, 569–581

43. van der Hoorn, R. a L., Leeuwenburgh, M. A., Bogyo, M., Joosten, M. H. A. J., and Peck, S. C. (2004) Activity Profiling of Papain-Like Cysteine Proteases in Plants. *Plant Physiol.* 135, 1170–1178

44. Weerapana, E., Speers, A. E., and Cravatt, B. F. (2007) Tandem orthogonal proteolysis-activity-based protein profiling (TOP-ABPP)--a general method for mapping sites of probe modification in proteomes. *Nat. Protoc.* 2, 1414–25

45. Michalski, a., Damoc, E., Lange, O., Denisov, E., Nolting, D., Muller, M., Viner, R., Schwartz, J., Remes, P., Belford, M., Dunyach, J.-J., Cox, J., Horning, S., Mann, M., and Makarov, a. (2012) Ultra High Resolution Linear Ion Trap Orbitrap Mass Spectrometer (Orbitrap Elite) Facilitates Top Down LC MS/MS and Versatile Peptide Fragmentation Modes. *Mol. Cell. Proteomics* 11, O111.013698-O111.013698

46. Olsen, J. V, de Godoy, L. M., Li, G., Macek, B., Mortensen, P., Pesch, R., Makarov, A., Lange, O., Horning, S., and Mann, M. (2005) Parts per million mass accuracy on an Orbitrap mass spectrometer via lock mass injection into a C-trap. *Mol Cell Proteomics* 4, 2010–2021

47. Cox, J., Neuhauser, N., Michalski, A., Scheltema, R. A., Olsen, J. V., and Mann, M. (2011) Andromeda: A peptide search engine integrated into the MaxQuant environment. *J. Proteome Res.* 10, 1794–1805

48. Cox, J., and Mann, M. (2008) MaxQuant enables high peptide identification rates, individualized p.p.b.-range mass accuracies and proteome-wide protein quantification. *Nat. Biotechnol.* 26, 1367–72

49. Cox, J., Hein, M. Y., Luber, C. a, and Paron, I. (2014) Accurate proteome-wide label-

free quantification by delayed normalization and maximal peptide ratio extraction, termed MaxLFQ. *Mol. Cell.* … 13, 2513–2526

50. Tyanova, S., Temu, T., Sinitcyn, P., Carlson, A., Hein, M. Y., Geiger, T., Mann, M., and Cox, J. (2016) The Perseus computational platform for comprehensive analysis of (prote)omics data. *Nat. Methods* 13, 731–40

51. Kammers, K., Cole, R., Tiengwe, C., and Ruczinski, I. (2015) Detecting significant changes in protein abundance. *EuPA open proteomics*, 11–19

52. Cruz, A. P. Z., Ferreira, V., Pianzzola, M. J., Siri, M. I., Coll, N. S., and Valls, M. (2014) A novel, sensitive method to evaluate potato germplasm for bacterial wilt resistance using a luminescent Ralstonia solanacearum reporter strain. *Mol. Plant. Microbe. Interact.* 27, 277–85

53. Almagro Armenteros, J. J., Sønderby, C. K., Sønderby, S. K., Nielsen, H., and Winther, O. (2017) DeepLoc: prediction of protein subcellular localization using deep learning. *Bioinformatics* 33, 3387–3395

54. Ilyas, M., Hörger, A. C., Bozkurt, T. O., Van Den Burg, H. A., Kaschani, F., Kaiser, M., Belhaj, K., Smoker, M., Joosten, M. H. A. J., Kamoun, S., and Van Der Hoorn, R. A. L. (2015) Functional Divergence of Two Secreted Immune Proteases of Tomato. *Curr. Biol.* 25, 2300–2306

55. French, E., Kim, B. S., Rivera-Zuluaga, K., and Iyer-Pascuzzi, A. S. (2017) Whole Root Transcriptomic Analysis Suggests a Role for Auxin Pathways in Resistance to Ralstonia solanacearum in Tomato. *Mol. Plant-Microbe Interact.* Accepted for publication (https://doi.org/10.1094/MPMI-08-17-0209-R)

56. Bellincampi, D., Cervone, F., and Lionetti, V. (2014) Plant cell wall dynamics and wall-related susceptibility in plant-pathogen interactions. *Front. Plant Sci.* 5, 228

57. Minic, Z., and Jouanin, L. (2006) Plant glycoside hydrolases involved in??cell wall

polysaccharide degradation. *Plant Physiol. Biochem.* 44, 435–449

58. Shabab, M., Shindo, T., Gu, C., Kaschani, F., Pansuriya, T., Chintha, R., Harzen, A., Colby, T., Kamoun, S., and van der Hoorn, R. A. L. (2008) Fungal Effector Protein AVR2 Targets Diversifying Defense-Related Cys Proteases of Tomato. *Plant Cell* 20, 1169–1183

59. Vailleau, F., Sartorel, E., Jardinaud, M.-F., Chardon, F., Genin, S., Huguet, T., Gentzbittel, L., and Petitprez, M. (2007) Characterization of the interaction between the bacterial wilt pathogen Ralstonia solanacearum and the model legume plant Medicago truncatula. *Mol. Plant. Microbe. Interact.* 20, 159–167

60. Digonnet, C., Martinez, Y., Denancé, N., Chasseray, M., Dabos, P., Ranocha, P., Marco, Y., Jauneau, A., and Goffner, D. (2012) Deciphering the route of Ralstonia solanacearum colonization in Arabidopsis thaliana roots during a compatible interaction: Focus at the plant cell wall. *Planta* 236, 1419–1431

61. Cravatt, B. F., Wright, A. T., and Kozarich, J. W. (2008) Activity-Based Protein Profiling: From Enzyme Chemistry to Proteomic Chemistry. *Annu. Rev. Biochem* 77, 383–414

62. Tian, M., Huitema, E., Da Cunha, L., Torto-Alalibo, T., and Kamoun, S. (2004) A Kazal-like extracellular serine protease inhibitor from Phytophthora infestans targets the tomato pathogenesis-related protease P69B. *J. Biol. Chem.* 279, 26370–26377

63. Jordá, L., Conejero, V., and Vera, P. (2000) Characterization of P69E and P69F, two differentially regulated genes encoding new members of the subtilisin-like proteinase family from tomato plants. *Plant Physiol.* 122, 67–74

64. Jordá, L., Coego, A., Conejero, V., and Vera, P. (1999) A genomic cluster containing four differentially regulated subtilisin- like processing protease genes is in tomato plants. *J. Biol. Chem.* 274, 2360–2365

65. Zuluaga, A. P., Solé, M., Lu, H., Góngora-Castillo, E., Vaillancourt, B., Coll, N., Buell, C. R., and Valls, M. (2015) Transcriptome responses to Ralstonia solanacearum infection in the roots of the wild potato Solanum commersonii. *BMC Genomics* 16, 246

66. Tornero, P., Conejero, V., and Vera, P. (1997) Identification of a new pathogen-induced member of the subtilisin-like processing protease family from plants. *J. Biol. Chem.* 272, 14412–14419

67. Tian, M., Benedetti, B., and Kamoun, S. (2005) A Second Kazal-like protease inhibitor from Phytophthora infestans inhibits and interacts with the apoplastic pathogenesis-related protease P69B of tomato. *Plant Physiol.* 138, 1785–93

68. Song, J., Win, J., Tian, M., Schornack, S., Kaschani, F., Ilyas, M., van der Hoorn, R. a L., and Kamoun, S. (2009) Apoplastic effectors secreted by two unrelated eukaryotic plant pathogens target the tomato defense protease Rcr3. *Proc. Natl. Acad. Sci. U. S. A.* 106, 1654–1659

69. Tian, M., Win, J., Song, J., Hoorn, R. Van Der, Knaap, E. Van Der, and Kamoun, S. (2007) A Phytophthora infestans Cystatin-Like Protein Targets a Novel Tomato Papain-Like Apoplastic Protease. *Plant Physiol.* 143, 364–377

70. Dixon, M. S., Golstein, C., Thomas, C. M., van Der Biezen, E. a, and Jones, J. D. (2000) Genetic complexity of pathogen perception by plants: the example of Rcr3, a tomato gene required specifically by Cf-2. *Proc. Natl. Acad. Sci. U. S. A.* 97, 8807–8814

71. Ishihara, T., Mitsuhara, I., Takahashi, H., and Nakaho, K. (2012) Transcriptome Analysis of Quantitative Resistance-Specific Response upon Ralstonia solanacearum Infection in Tomato. *PLoS One* 7,

72. Chepyshko, H., Lai, C.-P., Huang, L.-M., Liu, J.-H., and Shaw, J.-F. (2012)

Multifunctionality and diversity of GDSL esterase/lipase gene family in rice (Oryza sativa L. japonica) genome: new insights from bioinformatics analysis. *BMC Genomics* 13, 309

73. Oh, I. S., Park, A. R., Bae, M. S., Kwon, S. J., Kim, Y. S., Lee, J. E., Kang, N. Y., Lee, S., Cheong, H., and Park, O. K. (2005) Secretome analysis reveals an Arabidopsis lipase involved in defense against Alternaria brassicicola. *Plant Cell* 17, 2832–2847

74. Kwon, S. J., Jin, H. C., Lee, S., Nam, M. H., Chung, J. H., Kwon, S. Il, Ryu, C. M., and Park, O. K. (2009) GDSL lipase-like 1 regulates systemic resistance associated with ethylene signaling in Arabidopsis. *Plant J.* 58, 235–245

75. Lee, D. S., Kim, B. K., Kwon, S. J., Jin, H. C., and Park, O. K. (2009) Arabidopsis GDSL lipase 2 plays a role in pathogen defense via negative regulation of auxin signaling. *Biochem. Biophys. Res. Commun.* 379, 1038–1042

76. Hong, J. K., Choi, H. W., Hwang, I. S., Kim, D. S., Kim, N. H., Choi, D. S., Kim, Y. J., and Hwang, B. K. (2008) Function of a novel GDSL-type pepper lipase gene, CaGLIP1, in disease susceptibility and abiotic stress tolerance. *Planta* 227, 539–558

77. Vizcaíno, J. A., Csordas, A., Del-Toro, N., Dianes, J. A., Griss, J., Lavidas, I., Mayer, G., Perez-Riverol, Y., Reisinger, F., Ternent, T., Xu, Q. W., Wang, R., and Hermjakob, H. (2016) 2016 update of the PRIDE database and its related tools. *Nucleic Acids Res.* 44, D447–D456

Figure legends

Figure 1. *Ralstonia solanacearum* causes differential necrosis between cultivars. *A*, Necrotic lesions present in the leaves of infected Marmande and Hawaii 7996 plants 7 days

post-inoculation. ***B*,** Percentage of necrotic leaves according to a pre-defined necrotic symptoms scale. Three necrotic degrees were considered depending on the amount of affected surface: mild (< 25%), moderate (25-75%), and severe (>75%). ***C*,** Bacterial multiplication in the apoplast of Marmande and Hawaii 7996 leaves. Four independent leaves from three plants per variety were used for the quantification. Highlighted area indicates the day post-inoculation at which proteomic experiments were performed.

Figure 2. Hawaii 7996 shows enhanced apoplastic hydrolase activities in response to *R. solanacearum* infection. *A*, Papain-like cysteine proteases (*first panel*) and serine hydrolases (*second panel*) induced in the apoplast of Marmande and Hawaii 7996 tomato plants 2 days post-inoculation. 40 µl of apoplastic fluid obtained from mock- (-) and R. solanacearum-inoculated (+) Marmande (M) and Hawaii 7996 (H) plants were incubated either with (+) or without (-) the activity-based probes MV201 and FP to detect PLCP and SH activities, respectively. A non-probe sample using a mix of all apoplastic fluids (m) was loaded as a control. Labelling experiments were performed on three biological replicates, all showing the same protein profiles. ***B*,** Quantification of differential PLCP and SH activities highlighted (arrowhead) in *A* from three biological replicates (Fig. S6A) using the ImageQuant TL software. Error bars indicate ± standard error. Asterisks indicate statistical difference by t-test ($\alpha = 0.05$). AU, Arbitrary Units. ***C*,** Inhibition of PLCP and SH activities after pre-incubating apoplastic fluids from *R. solanacearum*-inoculated Hawaii 7996 plants either with (+) or without (-) specific protease inhibitors (E-64 for PLCPs, and a cocktail composed of DFP, DCI and PMSF for SHs) prior to labelling. A SYPRO® Ruby stained gel is shown as a loading control. The quantification of PLCP and SH activity inhibition has been normalized according to the corresponding loading control and is shown next to each gel.

Figure 3. Identification of differentially active PLCPs and SHs in response to *R. solanacearum*. *A-D,* Volcano plots summarizing the results from the statistical analysis. Logarithm of the adjusted p-values plotted against the logarithm of fold change (FC) of the conditions indicated in each graph. Comparisons are: ***A,*** susceptible Marmande vs tolerant Hawaii 7996 in mock conditions; ***B,*** the same varieties upon *R. solanacearum* infection; ***C,*** effect of infection on Marmande; and ***D,*** on Hawaii 7996 plants. Dashed lines indicate adjusted p-value = 0.05. Protein classes appear annotated using different colors. Other SH activities include: 1 esterase, 1 α/β hydrolase 2, 3 α/β hydrolase 6, 1 sialic acid-specific acetylesterase and 2 S28 serine carboxypeptidases, which were not detected significant in the test. PLCP, Papain-like cys protease; S8 SLP, subtilisin-like protease; S10 SCP, serine carboxypeptidase; PAE, pectinacetylesterase. ***E,*** Significantly activated/inhibited PLCPs and SHs (adjusted p-value < 0.05). Annotated names in the UniProtKB database are shown. Numbers inside *A-D* cells indicate $\log_2$ intensity fold changes among comparisons**.** Letters *A-D* correspond to comparisons *A-D* in the volcano plots.

Figure 4. Specific hydrolases are post-translationally activated upon *R. solanacearum* infection. *A,* Activity/abundance ratio for every protein in each experimental condition, calculated using $\log_2$ intensity values. Proteins distant from the diagonal are overrepresented upon *R. solanacearum* infection. ***B,*** Detailed $\log_2$ activity and abundance intensities for the three most distant proteins: O65836 (P69F), O65834 (P69C) and K4B8T8. Error bars indicate ± standard error of three biological replicates. Asterisks indicate activity or abundance significant differences upon infection by t-test (α = 0.05).

Figure 5. Variety-specific changes in apoplastic protein interactions upon *R. solanacearum* infection. Interaction networks for Marmande **(*A, B*)** and Hawaii 7996 **(*C, D*)**

plants were constructed as described in the *Experimental Procedures* section. Protein families were annotated using the STRING databases and highlighted with different colors. The oxidative stress response module contains proteins involved in glutathione metabolism, thioredoxins and other oxidative stress-related proteins (i. e. peroxidases).

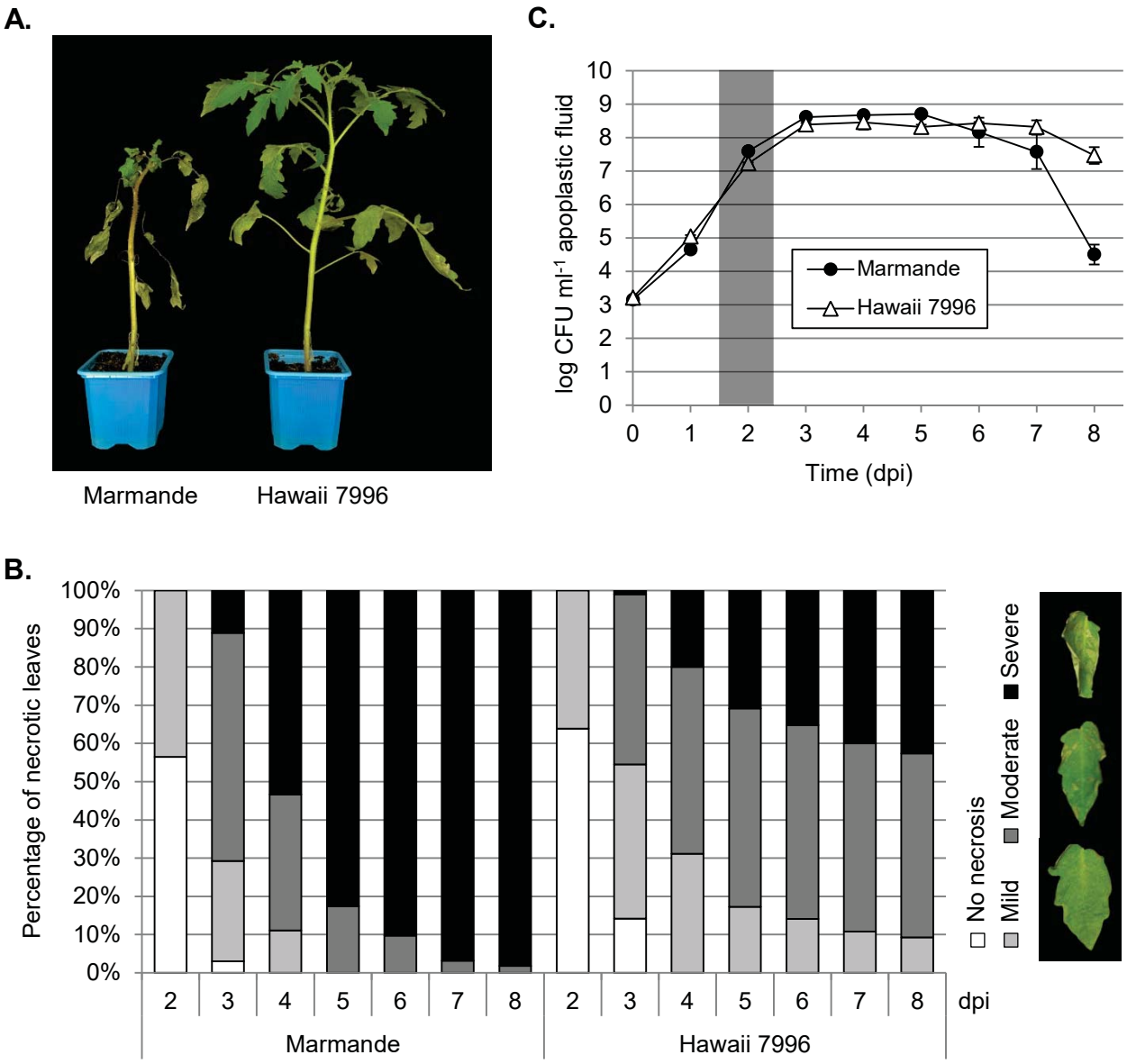

FIG. 1

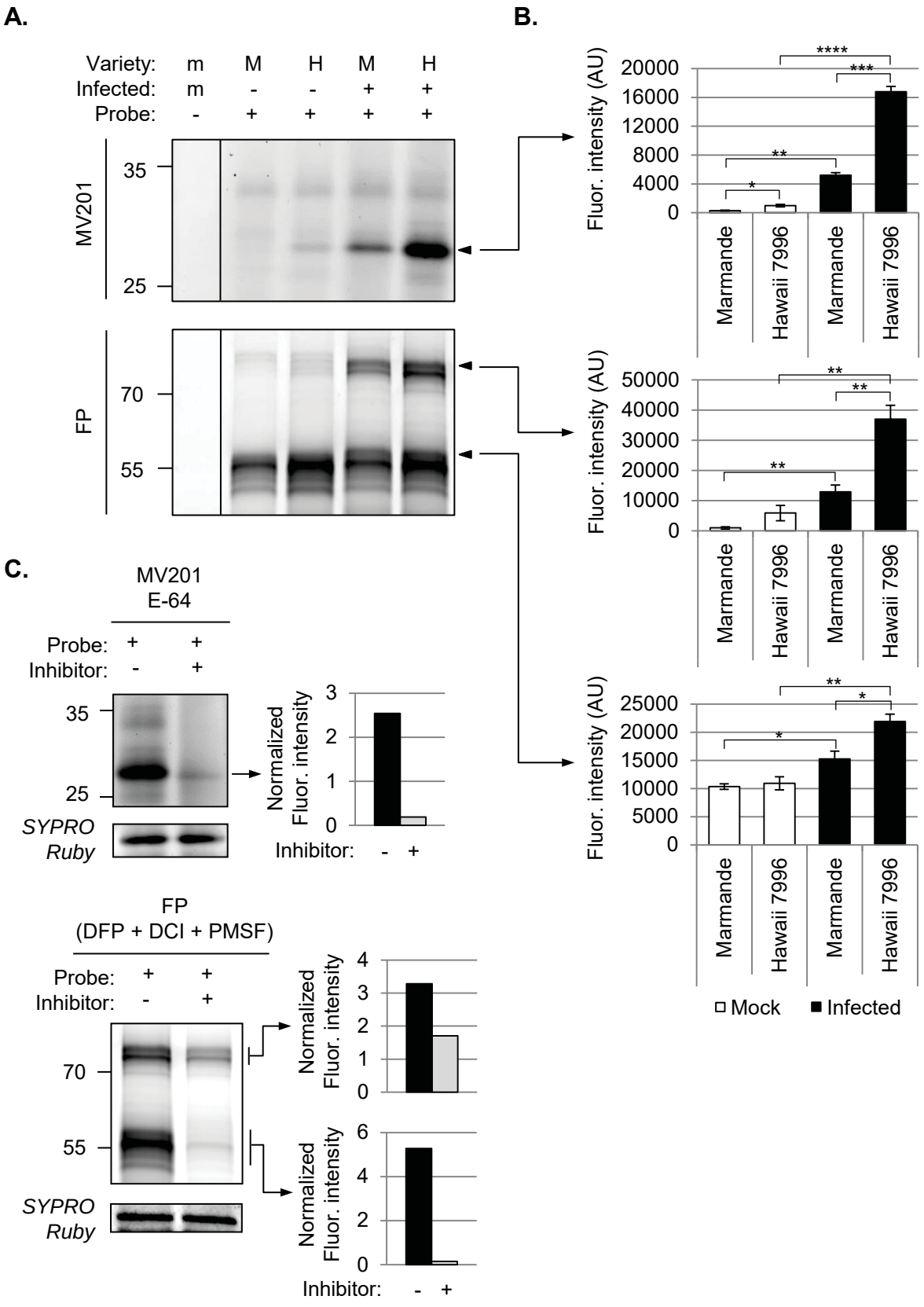

FIG. 2

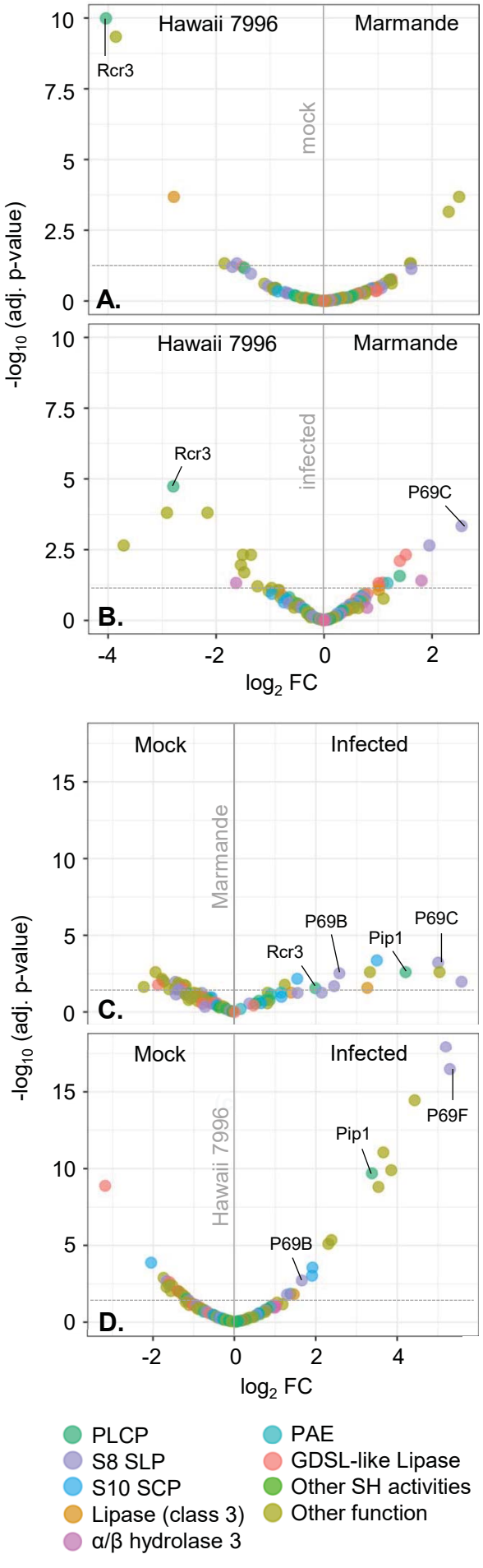

E.

Gene ID	UniProtKB ID (annotation)	MW [kDa]	Significant difference (FC)			
			A	B	C	D
Papain-like cys proteases *(family C1, clan CA)*						
Solyc02g076980.2.1	Q8S333 **(Rcr3)**	38.5	-4.0	-2.8	2.0	
Solyc02g077040.2.1	K4B8T1 **(Pip1)**	38.3			4.2	3.4
Solyc01g110110.2.1	K4B3M4	40.8				-1.2
Solyc07g041920.2.1	K4CE57	28.6		1.4		
Ser hydrolases						
Subtilases (family S8, clan SB)						
Solyc08g079900.1.1	K4CNZ0	79.5			5.6	5.2
Solyc08g079850.1.1	O65836 **(P69F)**	79.2				5.3
Solyc08g079880.1.1	O65834 **(P69C)**	80.1		2.6	5.0	
Solyc10g084320.1.1	K4D3L8	83.1		2.0		
Solyc08g079870.1.1	O04678 **(P69B)**	78.9			2.6	1.7
Solyc06g062950.1.1	K4C726	82.7				-1.7
Solyc08g079840.1.1	K4CNY4 **(PR-P69)**	79.0			2.5	1.3
Solyc08g079860.1.1	K4CNY6	79.2	-1.6			
Solyc12g088760.1.1	K4DGU7	81.0			-1.4	
Solyc04g078740.2.1	K4BUV9	81.1				-1.1
Solyc02g092670.1.1	K4BD63	80.0			-1.5	
Serine carboxypeptidase (family S10, clan SC)						
Solyc05g041540.2.1	K4C0D5	55.5			3.5	1.9
Solyc02g014830.2.1	K4B4T2	53.8				-2.1
Solyc01g108490.2.1	K4B364	58.0			1.5	1.9
Solyc06g083020.1.1	K4CAF7	55.9				1.4
Lipase (class 3)						
Solyc02g077110.2.1	K4B8T8	48.6	-2.8		3.3	
Solyc12g010910.1.1	K4DCH7	46.6				1.5
α/β hydrolase 3						
Solyc01g094010.2.1	K4AZE2	37.7		1.8		
Solyc02g069800.1.1	K4B7W2	37.2		-1.6		
Pectinacetylesterase						
Solyc08g005800.2.1	K4CI69	33.3		1.2		
GDSL-like Lipase						
Solyc01g100930.2.1	K4B1C4	41.1		1.4	-1.9	-3.2
Solyc03g005900.2.1	K4BE13	40.7		1.5		-1.4
Solyc02g071710.2.1	K4B8E7	41.7		1.1		-1.6
Solyc11g006250.1.1	G1DEX3 **(CD1)**	39.7		1.0		-1.1
Solyc03g121180.2.1	K4BMR7	39.0			-1.3	
Solyc01g079160.2.1	K4AXG2	40.6				-1.4
Solyc03g005910.2.1	K4BE14	40.1				-1.3

FIG. 3

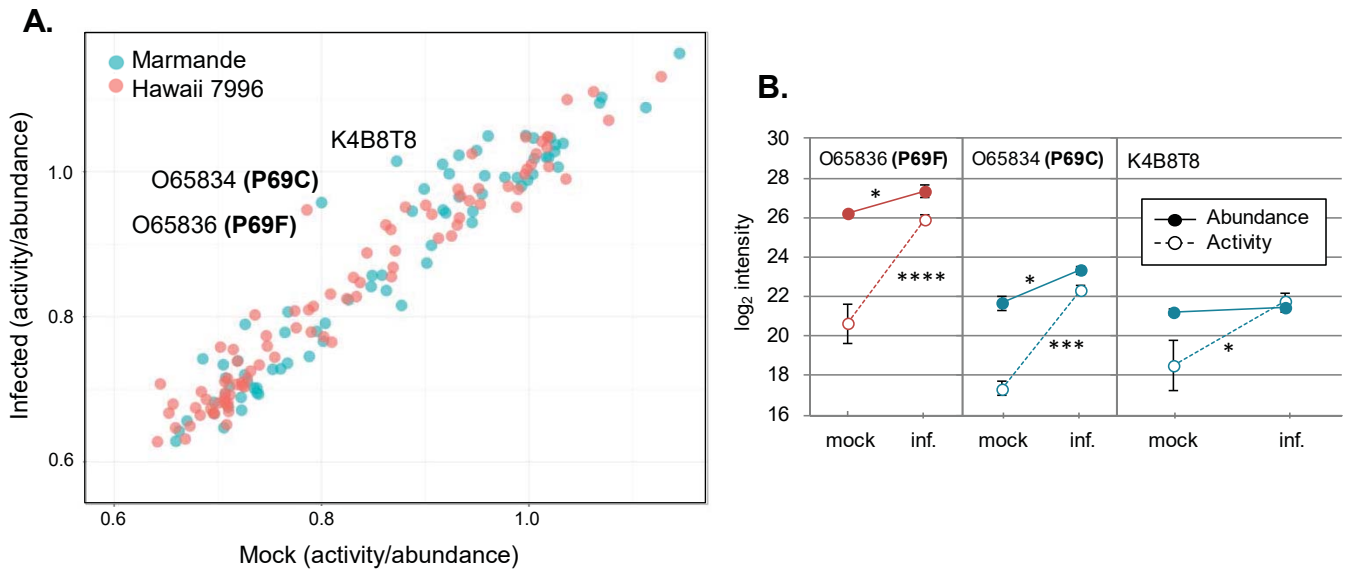

FIG. 4

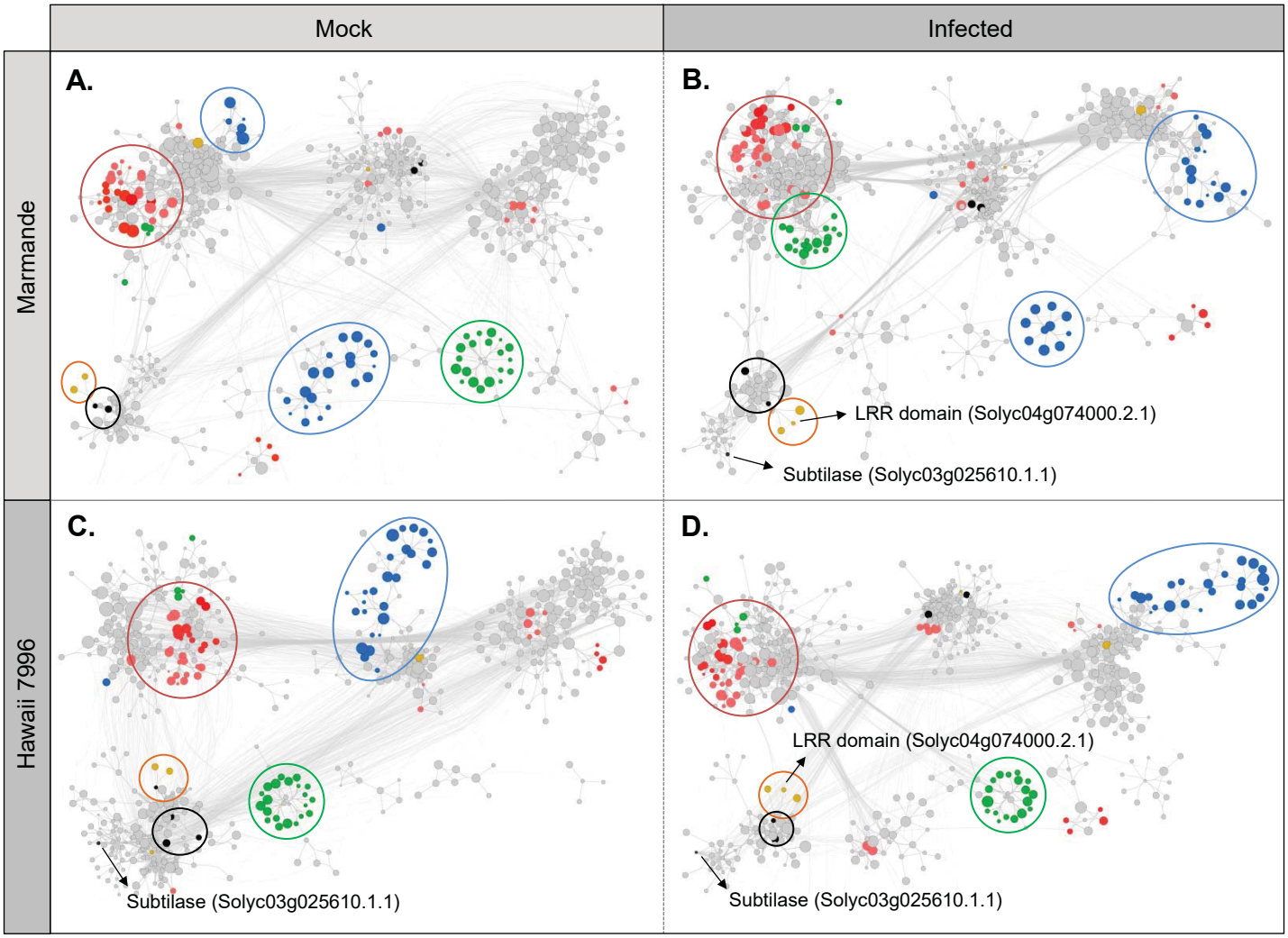

FIG. 5